An Efficient Buffering Mechanism for Mechanical Capturing Systems

Mohammadreza Alijani Nargesi[a], Reza Alibakhshi[b], Hassan Haddadpour[c,*], Kamran Daneshjou[d]

a. MSc, Department of Aerospace Engineering, Sharif University of Technology, Tehran, Iran.
b. PhD, Department of Mechanical Engineering, Iran University of Science and Technology, Tehran, Iran.
c. Professor, Department of Aerospace Engineering, Sharif University of Technology, Tehran, Iran.
d. Professor, Department of Mechanical Engineering, Iran University of Science and Technology, Tehran, Iran.

Abstract

Before implementing a mechanical capturing/coupling process between structures, collision occurs inevitably and the motion characteristics of a system may be significantly affected. The short time duration and the large force generated by impact leads to make the motion instability as well as to keep some probable embedded subsystems unprotected. To do this, it is aimed to propose an effective probe-cone buffering mechanism with capacity of impact energy dissipation in this article. To reduce the impact force and to provide the required protection of systems, probe including spherical tip mass is mounted on the active structure by the proposed buffer and cone on the passive one, as well. The kinetic effect of the tip mass is also investigated as an effective parameter on the proposed mechanism. By an example problem, the theoretical impact model is verified by data reported in the literature. Then, a virtual model is built by a commercial multibody dynamics analysis software to verify theoretical results and develop the proposed buffer. It will be shown herein that the proposed mechanism takes some advantages such as providing a remarkable decreasing effect on impact compared to the traditional rigid probe and performing the successful capture process in different coupling scenarios.

Keywords: Capturing systems; Effective buffering mechanism; Collision phenomenon; Impact dynamics; Multibody dynamics analysis

1. Introduction

Capturing process, exactly before making a rigid connection between two systems, is known as an essential function which is widely used in mechanical and aerospace applications. Constructing a new structure by assembling some components, stable connection and crashworthiness of rail vehicles, repairing malfunctioning components by the active vehicle and refueling aircraft by another tanker aircraft are examples in which capture process should be firstly and successfully executed. With the development of computer technology, the process of grasping or capturing a active object/structure become an important part of robotics task. Owing to this challenging mission, more and more research studies are required to create an accurate dynamic model before implementing in the real-world environment. Nowadays, the attention of researchers in capturing objects in many fields, from rail transportation to robotics and space industry, is significantly increasing. Here, some literatures related to applications of such mechanisms are reviewed. The various robotic locking mechanisms presented in literatures are investigated and compared to each other [1]. A self-locking mechanism which improves significantly the traction ability of robots is introduced [2]. The ability of damping impact energy can be critical in the rail vehicles coupling.

Therefore, a comprehensive study on passive railways crashworthiness has been conducted [3]. The stability of a high-speed rail vehicle under crosswind is investigated as well [4]. The dynamic analysis of a high-speed train collision with an obstacle is studied and an allowable maximum velocity has been proposed to ensure the safety of the occupants [5]. A case study on a city passenger train has been investigated using a multi-body dynamic formulation of a rigid body train. The observation showed that the proposed crashworthiness system can considerably reduce the impact energy [6]. In the same matter, a train collision state score is proposed which is capable to provide enough safety under the different impact conditions. Meanwhile, the influence of the energy absorbing was studied with respect to some important collision parameters. The results depict that the parameters such as initial height difference and pitching angle remarkably grow the train collision state score [7]. There are some literatures in which the dynamic behavior of the coupler during railways integration have been studied [8-10]. Recently, a novel method called Dynamic Coupling that permits physical coupling and decoupling of railway vehicles at cruising speeds was introduced [11]. The main factors noticed in capturing concept include: the location of contact point, the required internal force of manipulator gripper, the capturing mechanism connector torques and the stability of a passive vehicle. For these cases, there are some papers in which a number of objective functions have been optimized [12-14]. However, the main problem of such optimization processes is the long convergence time [15].

Impact force models can be classified into two main approaches. First, a continuous model where impact can be expressed by a function of indentation between the impacting objects. Second, a discrete model in which the dynamic analysis is divided into two parts namely before and after the collision. In fact, in this approach, the configuration of contacting bodies does not change obviously. Therefore, the first model takes advantage of simpler modeling because there is no need for calculations of impulse-momentum dynamics [16]. Also, impact force can be easily added to the equations of motion of the system [17]. To model a realistic impact force including the correlative terms such as energy dissipation during impact, many researchers have developed the Hertz contact law known as the first nonlinear continuous contact model [17-19]. Recently, some new continues contact model based on Hertz theory is introduced. The model is efficient for regular or irregular contacting surfaces [20] or even random surfaces [21]. Some extensive continues contact model is developed in different value of velocity and penetration [22]. The readers may consult the work [16,23] for more detail of other dissipative contact force theories.

The dynamic behavior of mechanisms, space structures and systems, railways coupling, vehicles and robotics are several examples of mechanical systems which can be modeled by constrained multibody dynamics. The numerical solution of the differential-algebraic equations (DAEs), due to their computational inefficiency in forward dynamics of multibody systems, is prone to errors [24] particularly for higher index systems and therefore, they are commonly converted to the set of ordinary differential equations (ODEs) and solved by a commonly used numerical integration algorithm [25]. Some useful details on the impact dynamic modeling in multibody systems can be found in [26]. Another capturing system based on probe-cone mechanism has been studied for spacecraft docking process in which the probe was rigidly mounted on active vehicle [27]. Compared to traditional capture systems [27], this part of the paper points out some advantages of the proposed buffer implementing successful capture process. First, by considering the suitable DOF for probe equipped with shock absorbers, not only lateral and rotational alignment of active vehicle with respect to the passive structure can be achieved but the equivalent mass of colliding objects can be passively controlled to decrease the maximum magnitude of impact force and to increase safety probability in the structure of two vehicles. Second, the proposed mechanism

resolves the difficulty of motion planning for a robotic arm connected to a passive vehicle. Third, to reduce the collision force and relative velocity between end point of the manipulator and contact point of the passive object, the proposed system does not require to an active controller design.
In this paper, an easy-to-install and effective buffering mechanism is proposed to successfully accomplish the capture process for two vehicles. The main advantage of this mechanism is in its efficiency during capture process where possible misalignment caused by manufacturing or other reasons. Furthermore, the present mechanism can remarkably reduce the impact force acting upon two vehicles. So, it can prevent the probable dangers or damages such as derailment phenomena. During capture process, the impact occurs and the nonlinear Lankarani-Nikravesh method is applied here to reflect an acceptable display of impact phenomenon with hysteresis damping. The active system is equipped with axial and torsional springs as shock absorbers that is more convenient mechanism performing the capture process and reducing the impact force without dependence on a control system. Owing to rotational symmetry of probe and cone, the problem is reasonably formulated as planar constrained multibody dynamics leading to the set of DAEs. A new technique is introduced to convert DAEs into ODEs by means of computer program. The correctness of the theoretical model will be verified by those reported in the literature. Also, a virtual model is built by a commercial multibody dynamics analysis software to verify results and develop the proposed buffer. To show the capability of proposed buffer, some coupling scenarios with different typical values are investigated. It will be demonstrated that the proposed buffering system not only has a remarkable decreasing effect on impact during collision but provides the successful capture in different misalignment angles and some other operation parameters. At the end, more decreasing effect of the mechanism in impact values has been investigated by considering the rotation of the tip mass with respect to the probe.

2. Proposed mechanism description

Capture process needs a physical contact between at least two objects, named active and passive vehicles. Figure 1 shows detail view on how all parts assembled together in the active vehicle. The probe is supposed to approach to the inner surface of the cone. For the restraint of the active vehicle with respect to passive one, some pre-loaded spring latches are mounted on the probe head, which can be engaged with corresponding catch on the cone's inner cylinder. Exerting compressive load by these pre-loaded spring latches leads the passive vehicle to be initially interlocked with another one to constraint their translational and rotational motions relative to each other. Here, the probe-cone system consists of an axial spring as a shock absorber located between the main body of the active vehicle and the end of probe. In this study, for the reason of stability, it is necessary to connect the base and active structure to each other using a torsional shock absorber. The conjunction between probe and active vehicle is created by two kinds of kinematic pairs. The motion of cylinder with respect to the active structure and the motion of probe relative to the base are limited by revolute joint and prismatic joint, respectively. Obviously, a 2-DOF probe can experience translational and rotational motions simultaneously with respect to the active vehicle during impact. Remarkable aspect of this proposed mechanism embedded into the active vehicle is to provide improvement regarding to the reduction of peak value of collision force as well as the equivalent colliding components prior to capture process. In fact, to gradually increase the equivalent mass instead of its rapid increasing in the impacting structures and to overcome the misalignment are the two main reasons for considering this type of mechanism.

3. Impact force model

Non-zero relative velocity in the case of collision leads to impact. Physically, the kinetic energy of body is suddenly lost during the impact and abrupt changes of the system state variables lead to discontinuities in the overall system velocities. Energy loss during impact, observed in the forms of heat, sound and others [28], depends on the damping properties of the materials involved in the collision. Here, the Lankarani and Nikravesh contact model, which is based on the Hertz contact theory, is applied to analysis the problem interactions. Equation 1 shows a parabolic distribution for collision force based on a continuous impact force model [18]:

$$F_n = \delta^{3/2}(K + \chi\dot{\delta}) \tag{1}$$

Where K is defined as the total stiffness. δ is the penetration depth evaluated by the problem geometry and $\dot{\delta}$ is the time derivative of penetration depth which is defined as the approaching velocity of the bodies in normal direction. The friction force due to normal force is assumed as $F_t = \mu F_n$ where μ is sliding friction coefficient and χ is the hysteresis damping factor which is defined as below [16]:

$$\chi = \frac{3K(1-e^2)}{4\dot{\delta}^{(-)}} \tag{2}$$

Where e is restitution coefficient and $\dot{\delta}^{(-)}$ is initial impact velocity in the normal direction, respectively. As can be seen from Figure 1, in the capture process, impact phenomenon happens between a ball head probe a cone. For this situation, the stiffness of the contact is obtained from the following relation [29]:

$$K = \frac{4\sqrt{R_{tip}}}{3(\sigma_{tip} + \sigma_{Cone})} \tag{3}$$

Where σ_{tip} and σ_{Cone} are the material parameters, as [30]:

$$\sigma_{tip} = \frac{1-\nu_{tip}^2}{E_{tip}}, \quad \sigma_{cone} = \frac{1-\nu_{cone}^2}{E_{cone}} \tag{4}$$

In which E and ν are the modulus of elasticity and Poisson's ratio of the bodies, respectively.

4. Multibody dynamics for capture process

In the planar analysis, it is observed that the most typical mechanical pairs used in the multibody systems are the revolute and prismatic joints. Accurate modeling of the multibody dynamic problems is created by coordinate systems placed on each object. For problem at hand, figure 2 shows all coordinate frames to describe the position of the system components. The body-fixed coordinate $[u_k, v_k, \theta_k]^T$ is located at the k-th body center. Here, subscripts S, C, P and T denote coordinates related to the passive structure, cylinder, probe and active vehicle, respectively. The vectors $\vec{r}_S$, $\vec{r}_C$, $\vec{r}_P$ and $\vec{r}_T$ may be simply written as:

$$\boldsymbol{r}_k = u_k\boldsymbol{i} + v_k\boldsymbol{j} \quad for \quad k = S,C,P,T \tag{5}$$

Although simple, the total kinetic energy of the constrained system can be written as:

$$T = 0.5\sum_{k=1}^{4}\left\{m_k\left(\dot{u}_k^2 + \dot{v}_k^2\right) + I_k\dot{\theta}_k^2\right\} \tag{6}$$

Where, m_k and I_k denote the mass and principal moment of inertia respectively. Figure 2 shows the coordinates frames during the capturing process. The parameters that involved in the capture process of two flying structures, are listed in Table 1. In the following, the theoretical model of the revolute joint and prismatic joint will be briefly described. According to the items in Table 1 and the iteration equation, two constrained equations for hinge and prism connectors are written. At each time step, the base and probe motion relative to each other should be restricted. For this, an auxiliary unit vector $\boldsymbol{n} = \{-\sin\theta_B, \cos\theta_B\}^T$, which must remain perpendicular to the line of translation, is introduced to eliminate relative translational motion. The above description gives four independent algebraic equations as below:

$$\begin{cases} u_S + a\cos\theta_S - u_B - 0.5L_C\cos\theta_C = 0 & \text{(7-a)} \\ v_S + a\sin\theta_S - v_B - 0.5L_C\sin\theta_C = 0 & \text{(7-b)} \end{cases}$$

$$\theta_C - \theta_P = 0\,, \tag{7-c}$$

$$\boldsymbol{n}\cdot(\boldsymbol{r}_P - \boldsymbol{r}_C) = 0\,. \tag{7-d}$$

For the sake of evaluation of the axial shock absorber performance, the auxiliary vector ($\boldsymbol{D}$) is defined to formulate the elastic potential and dissipative energy. In fact, this vector indicates the axial shock absorber length mounted between the end point of probe and an arbitrary point in the cylinder. Equation (8) defines $\boldsymbol{D}$ vector.

$$\boldsymbol{D} = \begin{pmatrix} u_P \\ v_P \end{pmatrix} - \begin{pmatrix} 0.5L_P\cos\theta_P \\ 0.5L_P\sin\theta_P \end{pmatrix} - \left(\begin{pmatrix} u_S \\ v_S \end{pmatrix} + \begin{pmatrix} a\cos\theta_S \\ a\sin\theta_S \end{pmatrix} - \begin{pmatrix} L_C\cos\theta_C \\ L_C\sin\theta_C \end{pmatrix}\right) \tag{8}$$

The summation of potential energy of linear and torsional shock absorbers is defined as below:

$$V = 0.5k_A\left(\|\boldsymbol{D}\| - l_0\right)^2 + 0.5k_T(\theta_C - \theta_S)^2 \tag{9}$$

In the above equation, $\|*\|$ indicates the two-norm operation. Additionally, k_A, k_T and l_0 are respectively the axial and torsional spring stiffnesses, and the equilibrium position of axial shock absorber. The Rayleigh dissipation function for the system under consideration can be written as:

$$P = 0.5c_A\dot{\boldsymbol{D}}\cdot\dot{\boldsymbol{D}} + 0.5c_T(\dot{\theta}_C - \dot{\theta}_S)^2 \tag{10}$$

In which, c_A and c_T are the viscous damping coefficients. It can be seen from Figure 3 that during the contact between two vehicles, two main forces, namely the normal force F_n in the direction perpendicular to the plane of cone and the tangential force F_t along the cone will occur. A suitable function for penetration depth seems to be defined in order to evaluate the impact force at each time step. For the reason of collision detection, first, the position of points *A*, *B* and *C* is written in

the global coordinate system and then, the penetration values are found by measuring the distance from point A to a specified line BC. The physical criteria to occur contact between two vehicles is negative values of the penetration depth during dynamic analysis procedure.

5. Problem formulation and computational strategy

The configuration of a dynamic constrained system in general form, with *k* generalized coordinates together with *m* constraints, may be formulated by the Lagrange's equation as:

$$\frac{d}{dt}\left(\frac{\partial T}{\partial \dot{\boldsymbol{q}}_k}\right)-\frac{\partial T}{\partial \boldsymbol{q}_k}+\frac{\partial V}{\partial \boldsymbol{q}_k}+\frac{\partial P}{\partial \dot{\boldsymbol{q}}_k}+\sum_{j=1}^{m}\boldsymbol{\lambda}_j a_{jk}=\boldsymbol{n}_k F_n+\boldsymbol{m}_k F_t \tag{11}$$

Where, $\boldsymbol{\lambda}_j$ and a_{jk} are the Lagrange's multipliers vector concerned with reaction forces/moments between interconnected components and the constraints equation coefficients, respectively. Also, $\boldsymbol{n}_k$ and $\boldsymbol{m}_k$ are the collision force coefficients. For simplicity, a similar expression of Eq. (11) is given here to rewrite corresponding equations of motion in the form of Newton's law of motion as below:

$$\frac{d}{dt}\left(\frac{\partial T}{\partial \dot{\boldsymbol{q}}_k}\right)=\boldsymbol{n}_k F_n+\boldsymbol{m}_k F_t-\boldsymbol{Re}_k \tag{12}$$

As can be seen, without considering the minimal set of coordinates, the system of Eq. (12) consists of *k* differential equations in *k+m* unknowns. Therefore, *m* additional equations are required to be augmented into the system of equations. Generally, when the constraint acceleration equations are appended to Eq. (12), the motion of multibody system can be written in matrix form as follows:

$$\begin{bmatrix}\boldsymbol{M} & \boldsymbol{\phi}_{\boldsymbol{q}}^{\boldsymbol{T}}\\ \boldsymbol{\phi}_{\boldsymbol{q}} & \boldsymbol{0}\end{bmatrix}\begin{Bmatrix}\ddot{\boldsymbol{q}}\\ \boldsymbol{\lambda}\end{Bmatrix}=\begin{Bmatrix}\boldsymbol{F}\\ \boldsymbol{\gamma}\end{Bmatrix} \tag{13}$$

Where $\boldsymbol{\phi}_q$ is the Jacobin matrix obtained by taking the derivative of the constraint equations and also γ defined as follows [18]:

$$\boldsymbol{\gamma}=-(\boldsymbol{\phi}_q\dot{\boldsymbol{q}})_q\dot{\boldsymbol{q}}-2\boldsymbol{\phi}_{qt}\dot{\boldsymbol{q}}-\boldsymbol{\phi}_{tt} \tag{14}$$

Due to the difficulties in the solution of a DAE system such as obtaining analytically inverted expression for equivalent mass matrix observed in the left side of Eq. (13) and violating the results caused by the set of inaccurate initial conditions in the integration process, this type of equations is commonly converted into a set of ODEs. Here, it is used an effective index-1 DAE solver, known as ode15s, taking advantage of automatically adjustment of step size in order to meet user-defined error as well as numerical stability during integration process. In general, the ode15s solver can evaluate the DAEs with the standard form given as $\boldsymbol{M}(t,\boldsymbol{y})\dot{y}=\boldsymbol{F}(t,\boldsymbol{y})$. Therefore, it is necessary to use an alternative reformulation to rewrite Eq. (13) into this general form. To specify the topology of system at hand, all involved coordinates have been assembled into the vector $\boldsymbol{q}=\{u_S,v_S,\theta_S,u_B,v_B,\theta_B,u_P,v_P,\theta_P,u_T,v_T,\theta_T\}^T$. Typically, in a system with *k* generalized coordinates, reducing the order of initial state variables leads to a new set of state variables by means of the standard change of variables as follows:

$$\dot{\boldsymbol{q}}_i = \boldsymbol{x}_i, i = 1,2,...,k \tag{15}$$

Reformulating Eq. (13) in view of Eq. (15) leads to:

$$\underbrace{\begin{bmatrix} \boldsymbol{I}_{k\times k} & \boldsymbol{0}_{k\times(k+m)} \\ \boldsymbol{0}_{(k+m)\times k} & \boldsymbol{M}^*_{(k+m)\times(k+m)} \end{bmatrix}}_{(2k+m)\times(2k+m)} \underbrace{\begin{Bmatrix} \dot{\boldsymbol{q}} \\ \dot{\boldsymbol{x}} \\ \boldsymbol{\lambda} \end{Bmatrix}}_{(2k+m)\times 1} = \underbrace{\begin{Bmatrix} \boldsymbol{x} \\ \boldsymbol{F}^* \\ \boldsymbol{\gamma}^* \end{Bmatrix}}_{(2k+m)\times 1} \tag{16}$$

Where $\boldsymbol{I}$ is the identity matrix. The superscript '*' is given here for presenting the problem reformulated with reduced-order state variables. Obviously, one can replace the vector λ by an arbitrary vector $\dot{\boldsymbol{\omega}}$ in the system of Eq. (16) to get general form of problem evaluated by the ode15s solver. By this technique, Eq. (16) can be expressed in the following simple from, as:

$$\boldsymbol{D(y)\dot{y} = F(y)} \tag{17}$$

In summary, the solution strategy for impact phenomenon is shown in Figure 4. Clearly, in this planar constrained model, the number of generalized coordinates and of constraint equations are, respectively, k=12 and m=4. So, the equivalent mass matrix has the dimension of 28×28. Also, the symmetric matrix $\boldsymbol{M}^*$ in the reduced form can be written as:

$$\boldsymbol{M}^* = \begin{bmatrix}
m_C & 0 & 0 & 0 & 0 & 0 & 0 & 0 & 0 & 0 & 0 & 0 & 0 & 1 & 0 & 0 & 0 \\
0 & m_C & 0 & 0 & 0 & 0 & 0 & 0 & 0 & 0 & 0 & 0 & 0 & 0 & 1 & 0 & 0 \\
0 & 0 & I_C & 0 & 0 & 0 & 0 & 0 & 0 & 0 & 0 & 0 & 0 & M^*_{3,13} & M^*_{3,14} & 0 & 0 \\
0 & 0 & 0 & m_B & 0 & 0 & 0 & 0 & 0 & 0 & 0 & 0 & 0 & -1 & 0 & 0 & M^*_{4,16} \\
0 & 0 & 0 & 0 & m_B & 0 & 0 & 0 & 0 & 0 & 0 & 0 & 0 & 0 & -1 & 0 & M^*_{5,16} \\
0 & 0 & 0 & 0 & 0 & I_B & 0 & 0 & 0 & 0 & 0 & 0 & 0 & M^*_{6,13} & M^*_{6,14} & 1 & M^*_{6,16} \\
0 & 0 & 0 & 0 & 0 & 0 & m_R & 0 & 0 & 0 & 0 & 0 & 0 & 0 & 0 & 0 & M^*_{7,16} \\
0 & 0 & 0 & 0 & 0 & 0 & 0 & m_R & 0 & 0 & 0 & 0 & 0 & 0 & 0 & 0 & M^*_{8,16} \\
0 & 0 & 0 & 0 & 0 & 0 & 0 & 0 & I_R & 0 & 0 & 0 & 0 & 0 & -1 & 0 & \\
0 & 0 & 0 & 0 & 0 & 0 & 0 & 0 & 0 & m_T & 0 & 0 & 0 & 0 & 0 & 0 & \\
0 & 0 & 0 & 0 & 0 & 0 & 0 & 0 & 0 & 0 & m_T & 0 & 0 & 0 & 0 & 0 & \\
0 & 0 & 0 & 0 & 0 & 0 & 0 & 0 & 0 & 0 & 0 & I_T & 0 & 0 & 0 & 0 & \\
1 & 0 & M^*_{13,3} & -1 & 0 & M^*_{13,6} & 0 & 0 & 0 & 0 & 0 & 0 & 0 & 0 & 0 & 0 & \\
0 & 1 & M^*_{14,3} & 0 & -10 & M^*_{14,6} & 0 & 0 & 0 & 0 & 0 & 0 & 0 & 0 & 0 & 0 & \\
0 & 0 & 0 & 0 & 0 & 1 & 0 & 0 & -1 & 0 & 0 & 0 & 0 & 0 & 0 & 0 & \\
0 & 0 & 0 & M^*_{16,4} & M^*_{16,5} & M^*_{16,6} & M^*_{16,7} & M^*_{16,8} & 0 & 0 & 0 & 0 & 0 & 0 & 0 & 0 &
\end{bmatrix} \tag{18}$$

Where,

$$\begin{aligned}
&M^*_{3,13} = -a\sin y(3), M^*_{3,14} = a\cos y(3), M^*_{4,16} = \sin y(6), M^*_{5,16} = \cos y(6) \\
&M^*_{6,13} = \left(\frac{L_C}{2}\right)\sin y(6), M^*_{6,14} = -\left(\frac{L_C}{2}\right)\cos y(6), \\
&M^*_{6,16} = (y(4) - y(7))\cos y(6) + (y(5) - y(8))\sin(y(6)), M^*_{7,16} = -\sin y(6) \\
&M^*_{8,16} = \cos y(6)
\end{aligned} \tag{19}$$

In view of Eq. (12), the force vector $\mathbf{F}^*$, as given in the right-hand side of Eq. (16), can be represented as:

$$\boldsymbol{F}^* = \boldsymbol{n}_k F_n + \boldsymbol{m}_k F_t - \boldsymbol{Re}_k \tag{20}$$

In which, $\boldsymbol{n}_k$ and $\boldsymbol{m}_k$ are given as:

$$\boldsymbol{n}_k = \begin{bmatrix} \boldsymbol{0}_{6\times1} \\ -sin(\beta + y_{12}) \\ cos(\beta + y_{12}) \\ \frac{L_P}{2} cos(\beta + y_{12} - y_9) \\ sin(\beta + y_{12}) \\ -cos(\beta + y_{12}) \\ b + L_T\, cos(\beta) + R_c\, sin(\beta) \end{bmatrix}, \boldsymbol{m}_k = \begin{bmatrix} \boldsymbol{0}_{6\times1} \\ -cos(\beta + y_{12}) \\ -sin(\beta + y_{12}) \\ -\frac{L_P}{2} sin(\beta + y_{12} - y_9) \\ cos(\beta + y_{12}) \\ sin(\beta + y_{12}) \\ R_c\, cos(\beta) - L_T\, sin(\beta) \end{bmatrix} \tag{21}$$

Because of inordinately long expressions for F_n and F_t, they have not been given here, $\boldsymbol{Re}_k$ which is concerned with *k*-th generalized coordinate (i.e., $Re_1, Re_2, \ldots, Re_{12}$) together with *m*-th constraint acceleration equation (i.e., $\mathrm{Re}_1, \mathrm{Re}_2, \ldots, \mathrm{Re}_{12}$), can be written in the reduced form, as below:

$$Re_1 = Re_2 = Re_{10} = Re_{11} = Re_{12} = Re_{15} = 0,$$

$$Re_3 = k_T(y(3) - y(6)) + c_T(y(15) - y(18)),$$

$$\begin{aligned} Re_4 = &-\frac{k_A\left(0.5L_C\, cos(y(6)) - 0.5L_P\, cos(y(9)) - y(4) + y(7)\right)\left(-l_0 + \sqrt{A}\right)}{\sqrt{A}} \\ &+0.5c_A\left(2y(16) - 2y(19) + L_C\, sin(y(6))y(18) - L_P\, sin(y(9))y(21)\right), \\ Re_5 = &-\frac{k_A\left(0.5L_C\, sin(y(6)) - 0.5L_P\, sin(y(9)) - y(5) + y(8)\right)\left(-l_0 + \sqrt{A}\right)}{\sqrt{A}} \\ &+0.5c_A\left(2y(17) - 2y(20) - L_C\, cos(y(6))y(18) + L_P\, cos(y(9))y(21)\right), \\ Re_6 = &\ 0.25\frac{k_A L_C B\left(-l_0 + \sqrt{A}\right)}{\sqrt{A} + k_T(y(6) - y(3)) + c_T(y(18) - y(15))} \\ &+0.25c_A L_C\left(2\, sin(y(6))(y(16) - y(19))\right) - 2\, cos(y(6))(y(17) - y(20)) + L_C y(18) \\ &-L_P\, cos(y(6) - y(9))y(21), \end{aligned} \tag{22}$$

$$Re_7 = \frac{k_A\left(0.5L_C\, cos(\,y(6)) - 0.5L_P\, cos(\,y(9)) - y(4) + y(7)\right)\left(-l_0 + \sqrt{A}\right)}{\sqrt{A}}$$
$$-0.5c_A\left(2y(16) - 2y(19) + L_C\, sin(\,y(6))y(18) - L_P\, cos(\,y(9))y(21)\right),$$
$$Re_8 = \frac{k_A\left(0.5L_C\, sin(\,y(6)) - 0.5L_P\, sin(\,y(9)) - y(5) + y(8)\right)\left(-l_0 + \sqrt{A}\right)}{\sqrt{A}}$$
$$-0.5c_A\left(2y(17) - 2y(20) - L_C\, cos(\,y(6))y(18) + L_P\, cos(\,y(9))y(21)\right),$$
$$Re_9 = -0.25\frac{k_A L_P B\left(-l_0 + \sqrt{A}\right)}{\sqrt{A}} + 0.25c_A L_P\left(2\, sin(\,y(9))(\,y(19) - y(16))\right)$$
$$+2\, cos(\,y(9))(\,y(17) - y(20)) + L_P y(21)$$
$$-L_C\, cos(\,y(6) - y(9))y(18),$$
$$Re_{13} = \frac{L_C}{2}\, cos(\,y(6))(\,y(18))^2 - a\, cos(\,y(3))(\,y(15))^2,$$
$$Re_{14} = \frac{L_C}{2}\, sin(\,y(6))(\,y(18))^2 - a\, sin(\,y(3))(\,y(15))^2$$
$$Re_{16} = y(18)(2\, cos(\,y(6))(\,y(16) - y(19))) + 2\, sin(\,y(6))(\,y(17) - y(20))$$
$$+y(18)\, sin(\,y(6))(\,y(7) - y(4)) + y(18)\, cos(\,y(6))(\,y(5) - y(8))$$

In which *A* and *B* are defined as:

$$A = \left(0.5L_C\, cos(\,y(6)) - 0.5L_P\, cos(\,y(9)) - y(4) + y(7)\right)^2$$
$$+\left(0.5L_C\, sin(\,y(6)) - 0.5L_P\, sin(\,y(9)) - y(5) + y(8)\right)^2, \qquad (23)$$
$$B = L_P\, sin(\,y(6) - y(9)) + 2\, sin(\,y(6))(\,y(4) - y(7)) + 2\, cos(\,y(6))(\,y(8) - y(5)).$$

6. Capture process simulation using commercial dynamics software

Dynamics evaluation can be carried out by simulation and/or alternatively by real experiments. In the case of capture process, the computer dynamic simulation can be used as an advantageous tool in testing the mechanical systems due to the low-cost need for components to be manufactured. Hence, the aim of this section is to establish a virtual model for capture process of two impacting/capturing structures based on the dynamic analysis software which can create and analysis a wide range of the multibody mechanical systems. To simulate the capture process, a three-dimensional solid model, as depicted in Figure 5, is established and then, the impact between the active and passive vehicles is simulated through software. Whether the capture process is successfully performed or not can be identified by employing a distance sensor located between the tip mass and the inner edge of the concave area. Evidently, the zero value of the sensor indicates the successful capture mission. The simulation time step is set to $\Delta t = 1\times10^{-5}\, s$ and the sliding friction coefficient is assumed as 0.33.

7. Numerical scheme and discussion

To ascertain the efficiency of the simulated and numerical models, the verification is performed using the available data reported in the literature and the software simulation. Required parameters for capture simulation, are summarized in Table 2 and also, material of both the active and passive vehicles are assumed to be aluminum alloy. Young's modulus, density and Poisson's ratio are $71.7\times10^{9}\,\mathrm{N/m^2}$, $2740\,\mathrm{kg/m^3}$ and 0.3, respectively. To examine the validity of the calculated results, it is applied available impact data reported in the literature [27]. Due to lack of any data on impact analysis during capture process, we have paid our attention to special case related to space docking process. To do this, the coefficients of the proposed buffer are postulated high enough to prevent translational and rotational motions of the probe with respect to active vehicle (i.e. rigid connection). Figure 6 indicates the impact force of two vehicles in the absence of the proposed mechanism. As observed from Figure 6, there is a very good agreement between the presented model and those yielded theoretically and experimentally in the literature. For the sake of comparative study between numerical results obtained by theoretical model and the dynamics analysis software, the axial and torsional shock absorber coefficients are set to be $k_A = 500\,\mathrm{N/m}, c_A = 5\,\mathrm{Ns/m}$ and, $k_T = 300\,\mathrm{Nm/rad}, c_T = 2\,\mathrm{Nms/rad}$ respectively. Also, l_0 (the initial length of the buffer) and M_B, as the cylinder mass are assumed to be $0.1365m$ and $1kg$. The relative velocity between the active and passive vehicles is considered as $0.1m/s$. Figure 7 illustrates impact force with the presence of the present mechanism based on theoretical model and software simulation. It can be concluded that the buffering mechanism performs a drastic cut in impact intensity during the collision phenomena. Comparing the data obtained by multibody dynamics model and those simulated by dynamics analysis software, a satisfactory similarity is observed. The proposed buffering system causes the mass of colliding objects to increase slowly and therefore, enhances the collision time during the impact process. The computed time history velocity components are shown based on the theoretical model and software simulation for both vehicles in Figure 8. There is an excellent agreement between results calculated by the numerical model and those simulated by the multi-body dynamic analysis software.

The performance of axial and torsional buffers during the impact is plotted in Figure 9. The buffer is unstretched at initial time and during impact, they are compressed and then came back to its initial length at the end of contact. As observed in Figure 9, the results simulated through the dynamics analysis software are consistent with those yielded by theoretical model formulated in this study.

8. Parametric study on efficient factors

This section is related to the study of effective factors showing whether the proposed buffer is able to implement successful capture process or not. To present the efficiency of mechanism, each proposed capture system should be able to successfully implement process for typical values of capturing, which are: the approach velocity of the active vehicle, the passive vehicle angular velocity, relative angular misalignment and friction coefficient. Keeping in mind that upon entering the probe head into capture area, the latches will engage the corresponding catch installed on passive vehicle (see Figure 1). A distance sensor as a distance criterion has been located between the tip of the probe and the inner edge of the cone. Provided that this criterion approaches to zero during simulation, the capture process will be successfully performed. The capability of the proposed mechanism in successful capture process is depicted in Figure 10. As observed, the higher the approach velocity is, the shorter the contact duration is. Note that the proposed buffer

not only has a remarkable decreasing effect on impact force but provides the successful capture mission for operational values of approach velocity. Another parameter to be evaluated in capture process is angular velocity of the passive vehicle. As shown in Figure 11, the proposed mechanism is able to reach capture area for different values of the passive vehicle's angular velocity (0, 0.05, 0.1*deg/s*). Because the angular misalignment of two capturing vehicles is an evident factor, each proposed coupling mechanism should be able to implement capture process correctly. The efficiency of proposed system in capture process for different values of angular misalignment is illustrated in Figure 12. With a suitable mass and spring system installed on the active vehicle, probe head can easily slide on the cone surface without perfect rebound and consequently, the distance criterion approaches to zero. One the main parameters to guarantee the successful capture execution is friction coefficient between head of probe and cone surface. To study this, five cases with the same initial approach velocity of 0.1*m/s* are modeled to investigate the effect of friction coefficient on contact duration. As plotted in Figure 13, the proposed system can achieve the capture area for various friction coefficients. The obtained results clearly indicate that increasing the value of friction coefficient leads to increase the total contact duration. The rotation of tip mass with respect to the probe is the next factor considered here. Let us consider the tip mass is rigidly connected to the end of probe according to above theoretical formulation (first case) and it is allowed to be freely rotate during contact with inner surface of the cone based of multibody dynamics software (second case). As depicted in Figure 14, in the second case, the maximum impact force decreased by 7% compared to the first case. In the second case, the tip mass experiences both sliding and rolling motions while it has just sliding motion in the first case. Because of rolling motion, the friction force generated at the area of contact decreases and consequently, the contact duration, penetration depth and resultant impact force decrease. In the second case, it will be studied some factors which directly show the efficiency of the proposed buffer in the capture process based on software simulation.

The capture process is successfully accomplished for different approach velocities of active vehicle, as depicted in Figure 15. According to Figure 16 and Figure 17, the present buffer is able to correctly perform capture process at different angular velocities and the misalignment angles of the passive vehicle. It is noteworthy to mention that, based on the obtained results, the capture process has been accomplished faster while tip mass experiences rolling-sliding motion instead of traditional pure sliding motion. As a consequence, the proposed buffering mechanism includes a compact structure with capacity of significant decreasing effect on impact and easy installation on a wide range of mechanical systems to be captured by each other.

9. Concluding remarks

An effective buffering mechanism was proposed based on probe-cone system for capture process of two impacting structures in this study. The constrained multibody dynamics model was used to derive equations of motion as the set of DAEs. To overcome the difficulties in evaluating DAEs, an easy-to-handle index-1 DAE solver was applied to solve the corresponding equations. The theoretical impact model is first verified by data reported in the literature. Second, the capture

process was built in the virtual prototype environment through commercial multibody dynamics analysis software in order to verify theoretical model and to develop proposed buffer. As shown, the numerical results obtained by theoretical model were in a very good agreement with those yielded through the dynamic simulation software. Compared to the traditional rigid connection of probe to the active vehicle, the simulation example indicated that the proposed buffer can greatly reduce the impact force and successfully perform the coupling of two vehicles for different values of effective factors arising from the capture process.

References

[1] Plooij, M., Mathijssen, G., Cherelle, P., et al., "Lock Your Robot: A Review of Locking Devices in Robotics", IEEE Robotics & Automation Magazine, **22**(1), pp. 106-117, (2015). https://doi.org/10.1109/MRA.2014.2381368

[2] Qiao, J., Shang, J., and Goldenberg A. "Development of inchworm in-pipe robot based on self-locking mechanism", IEEE/ASME Transactions On Mechatronics, **18**(2), pp. 799-806, (2012). https://doi.org/10.1109/TMECH.2012.2184294

[3] Zhu, T., Xiao, S., Lei, C., et al., "Rail vehicle crashworthiness based on collision energy management: an overview", International Journal of Rail Transportation, **9**(2), pp. 101-131, (2021). https://doi.org/10.1080/23248378.2020.1777908

[4] Li, D., Song, H., Meng, G., et al., "Dynamic characteristics of wheel–rail collision vibration for high-speed train under crosswind", Vehicle System Dynamics, **61**(8), pp. 1997-2022, (2023). https://doi.org/10.1080/00423114.2022.2093761

[5] Yao, S., Kong, L., Xu, P., et al., "Investigation on the dynamic characteristic of occupant during the frontal collision between high-speed train and obstacle", Accident Analysis & Prevention, **199**, pp. 107495, (2024). https://doi.org/10.1016/j.aap.2024.107495

[6] Wang, Y., Zhao, L., Cai, X., et al., "Dynamic damage evolution of double-block ballastless track structure under train derailment impact", Engineering Failure Analysis, **162**, pp. 108347, (2024). https://doi.org/10.1177/168781402110043

[7] Li, Z., Zhu, T., and Xiao, S. "Study on the Frontal Collision Safety of Trains Based on Collision Dynamics", Applied Sciences, **13**(19), pp. 10805, (2023). https://doi.org/10.3390/app131910805

[8] Yadav, O.P., and Vyas, N. S. "The influence of AAR coupler features on estimation of in-train forces", Railway Engineering Science, **31**(3), pp. 233-251, (2023). https://doi.org/10.1007/s40534-022-00297-8

[9] Zhang, J., Zhu, T., Yang, B., et al., "A rigid–flexible coupling finite element model of coupler for analyzing train instability behavior during collision", Railway Engineering Science, **31**(4), pp. 325-339, (2023). https://doi.org/10.1007/s40534-023-00308-2

[10] Wu, Q., Ge, X., Han, Q. L., et al., "Dynamics and control simulation of railway virtual coupling", Vehicle System Dynamics, **61**(9), pp. 2292-2316, (2023). https://doi.org/10.1080/00423114.2022.2105241

[11] Wu, Q., Ge, X., Zhu, S., et al., "Physical coupling and decoupling of railway trains at cruising speeds: train control and dynamics", International Journal of Rail Transportation, **12**(2), pp. 217-232, (2024). https://doi.org/10.1080/23248378.2023.2169963

[12] Watanabe T., and Yoshikawa, T. "Optimization of grasping by using a required external force set", Journal of the Robotics Society of Japan, **21**(3), pp. 321-326, (2003). https://doi.org/10.7210/jrsj.21.321

[13] Mangialardi, L., Mantriota G., and Trentadue, A. "A three-dimensional criterion for the determination of optimal grip points", Robotics and Computer-integrated manufacturing, **12**(2), pp. 157-167, (1996). https://doi.org/10.1016/0736-5845(96)00001-4

[14] Ito, S., Takeuchi, S., and Sasaki, M. "Object orientation in two dimensional grasp with friction towards minimization of gripping power", Biological cybernetics, **101**, pp. 215-226, (2009). https://doi.org/10.1007/s00422-009-0331-8

[15] Lampariello, R., Nguyen-Tuong, D., Castellini, C., et al., "Trajectory planning for optimal robot catching in real-time", 2011 IEEE International Conference on Robotics and Automation, IEEE, pp. 3719-3726, (2011). https://doi.org/10.1109/ICRA.2011.5980114

[16] Flores, P., and Lankarani, H. M. "Contact force models for multibody dynamics", Springer, **226** (2016). https://doi.org/10.1007/978-3-319-30897-5

[17] Lankarani, H. M., and Nikravesh, P. "A contact force model with hysteresis damping for impact analysis of multibody systems", International design engineering technical conferences and computers and information in engineering conference, American Society of Mechanical Engineers, **3691**, pp. 45-51, (1989). https://doi.org/10.1115/1.2912617
[18] Hunt, K. H., and Crossley, F. R. E. "Coefficient of restitution interpreted as damping in vibroimpact", (1975). https://doi.org/10.1115/1.3423596
[19] Safaeifar, H., and Farshidianfar, A. "A new model of the contact force for the collision between two solid bodies", Multibody System Dynamics, **50**, pp. 233-257, (2020). https://doi.org/10.1007/s11044-020-09732-2
[20] Zhang, J., Li, W., Zhao, L., et al., "A continuous contact force model for impact analysis in multibody dynamics", Mechanism and Machine Theory, **153**, pp. 103946, (2020). https://doi.org/10.1016/j.mechmachtheory.2020.103946
[21] Ta, W., Qiu, S., Wang, Y., et al., "Volumetric contact theory to electrical contact between random rough surfaces", Tribology International, **160**, pp. 107007, (2021). https://doi.org/10.1016/j.triboint.2021.107007
[22] Zhang, J., Liang, X., Zhang, Z., et al., "A continuous contact force model for impact analysis", Mechanical Systems and Signal Processing, **168**, pp. 108739, (2022). https://doi.org/10.1016/j.ymssp.2021.108739
[23] Stronge, W. J. "Impact mechanics", Cambridge university press, (2018). https://doi.org/10.1017/CBO9780511626432
[24] Marques, F., Souto A. P., and Flores, P. "On the constraints violation in forward dynamics of multibody systems", Multibody System Dynamics, **39**, pp. 385-419, (2017). https://doi.org/10.1007/S11044-016-9530-Y
[25] Shampine, L. F. "Computer solution of ordinary differential equations", The initial value problem, (1975). https://archive.org/details/computersolution0000sham
[26] Khulief, Y. "Modeling of impact in multibody systems: an overview", Journal of Computational and Nonlinear Dynamics, **8**(2), pp. 021012, (2013). https://doi.org/ 10.1115/1.4006202
[27] Zhang, X., Huang, Y., Han, W., et al., "Research of flexible beam impact dynamics based on space probe-cone docking mechanism", Advances in Space Research, **49**(6), pp. 1053-1061, (2012). https://doi.org/101016/j.asr.2011.12.030
[28] Gilardi, G., and Sharf, I. "Literature survey of contact dynamics modelling", Mechanism and Machine Theory, **37**(10), pp. 1213-1239, (2002). https://doi.org/10.1016/S0094-114X(02)00045-9
[29] Flores, P., Ambrósio, J., Claro, J., et al., "Translational joints with clearance in rigid multibody systems", (2008). https://doi.org/10.1115/1.2802113
[30] Goldsmith, W., and Frasier, J. T., "Impact: the theory and physical behaviour of colliding solids", (1960). https://doi.org/10.1115/1.3641808

Biographies

Mohammadreza Alijani Nargesi received his BSc and MSc degrees, both in Aerospace Engineering, from Sharif University of Technology, Iran, in 2016 and 2018, respectively. He is currently a PhD student at Amirkabir university of Technology. His main research interests are multibody dynamics, aeroelasticity and finite element methods.

Reza Alibakhshi received his MSc degree (Mechanical Engineering) from Babol University of Technology in 2010 and PhD degree from Iran University of Science and Technology in 2018. His research interests are multibody dynamics formulation, computational mechanics, mechanisms design and simulation.

Hassan Haddadpour received his MSc and PhD degrees, both from Department of Mechanical Engineering, University of Tehran, Iran, in 1996, and 2002, respectively. He is currently Professor at the department of aerospace engineering, Sharif University of Technology, Iran. His main

research interests are aeroelasticity, computational multibody dynamics, reduced order modeling, structural design of aerospace vehicles, aeroservoelasticity, structural dynamics and optimization.

Kamran Daneshjou received his BSc and MSc degrees (Mechanical Engineering) from Queen Mary College and Imperial College of London, respectively. He also received his PhD degree from Amirkabir University of technology. He is currently professor at the department of mechanical engineering, Iran University of Science and Technology. His research interests includes structural dynamics, spacecraft mechanisms design and systems identification.

List of Figure captions

List of Table captions

Table 1

Parameter	Description
a	Distance between CG point of active vehicle and clamped end of probe
L_C	Cylinder length
L_P	Probe length
L_T	Distance between cone and CG point of passive vehicle
b	Distance between cone and initial contact point
R_c	Radius of cone
R_{tip}	concentrated mass radius
L_c	Cone length
β	Angle of cone area
r_P	Ball radius

Table 2

active vehicle	passive vehicle
$m_S = 21.9706\ kg$	$m_T = 23.5731\ kg$
$I_S = 0.445\ kg.m^2$	$I_T = 0.5206\ kg.m^2$
$r_P = 0.009\ m$	$L_T = 0.096\ m$
$R_{tip} = 0.015\ m$	$R_c = 0.015\ m$
$a = 0.1365\ m$	$L_c = 0.0735\ m$
$L_P = 0.2\ m$	$b = 0.0435\ m$
$L_C = 0.1365\ m$	$\beta = \pi/4\ rad$

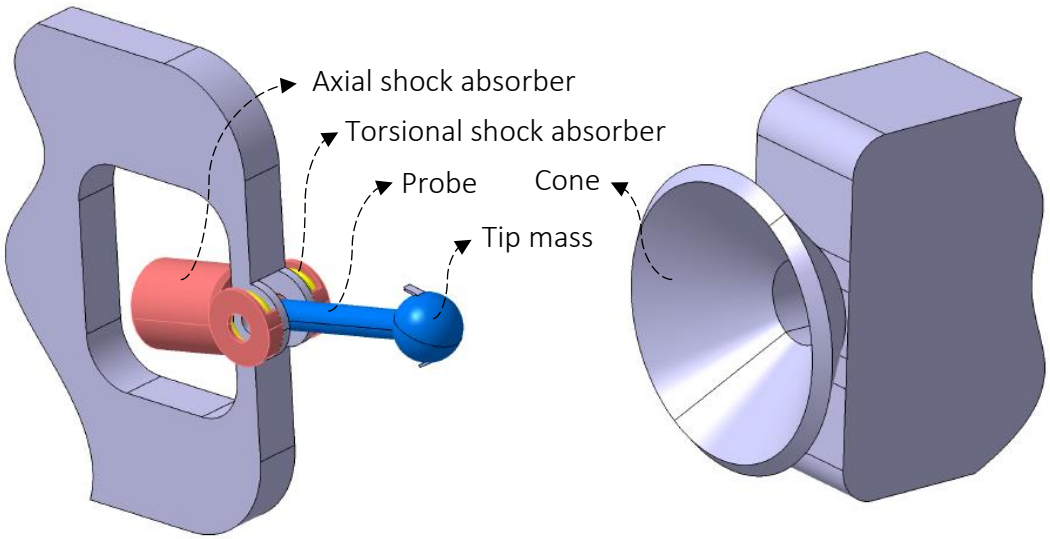

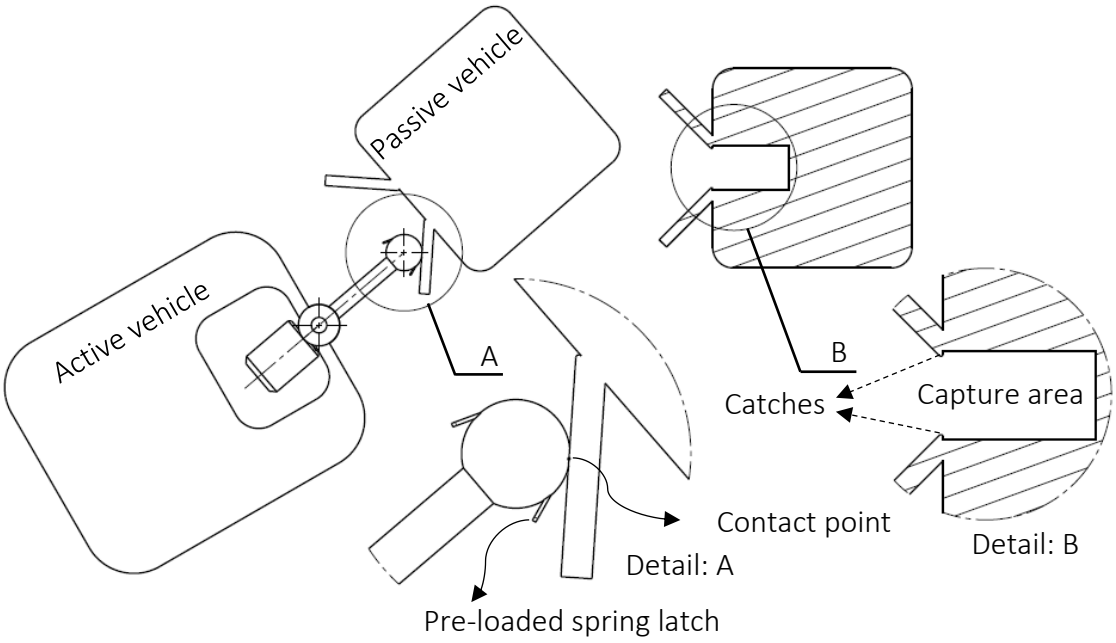

Figure 1

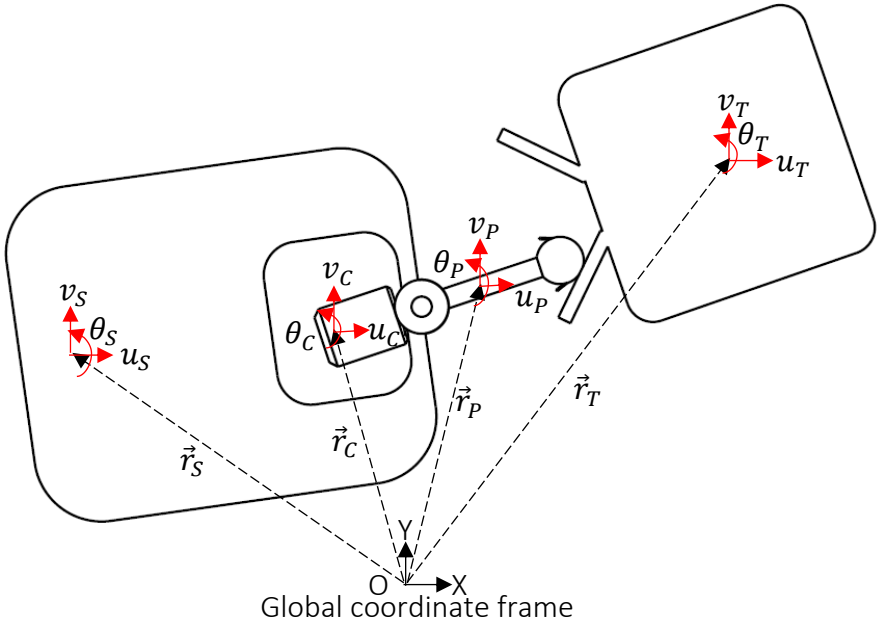

Figure 2

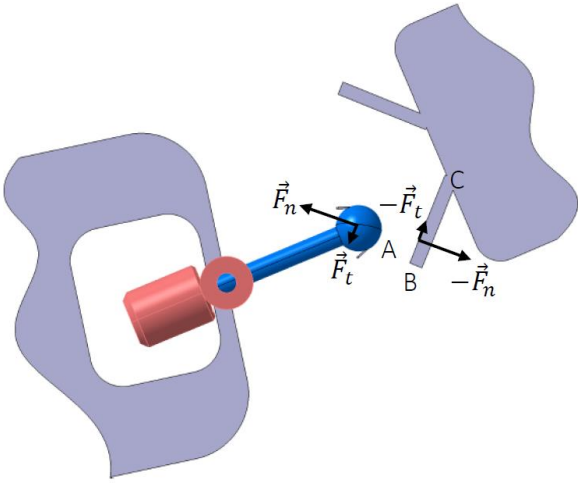

Figure 3

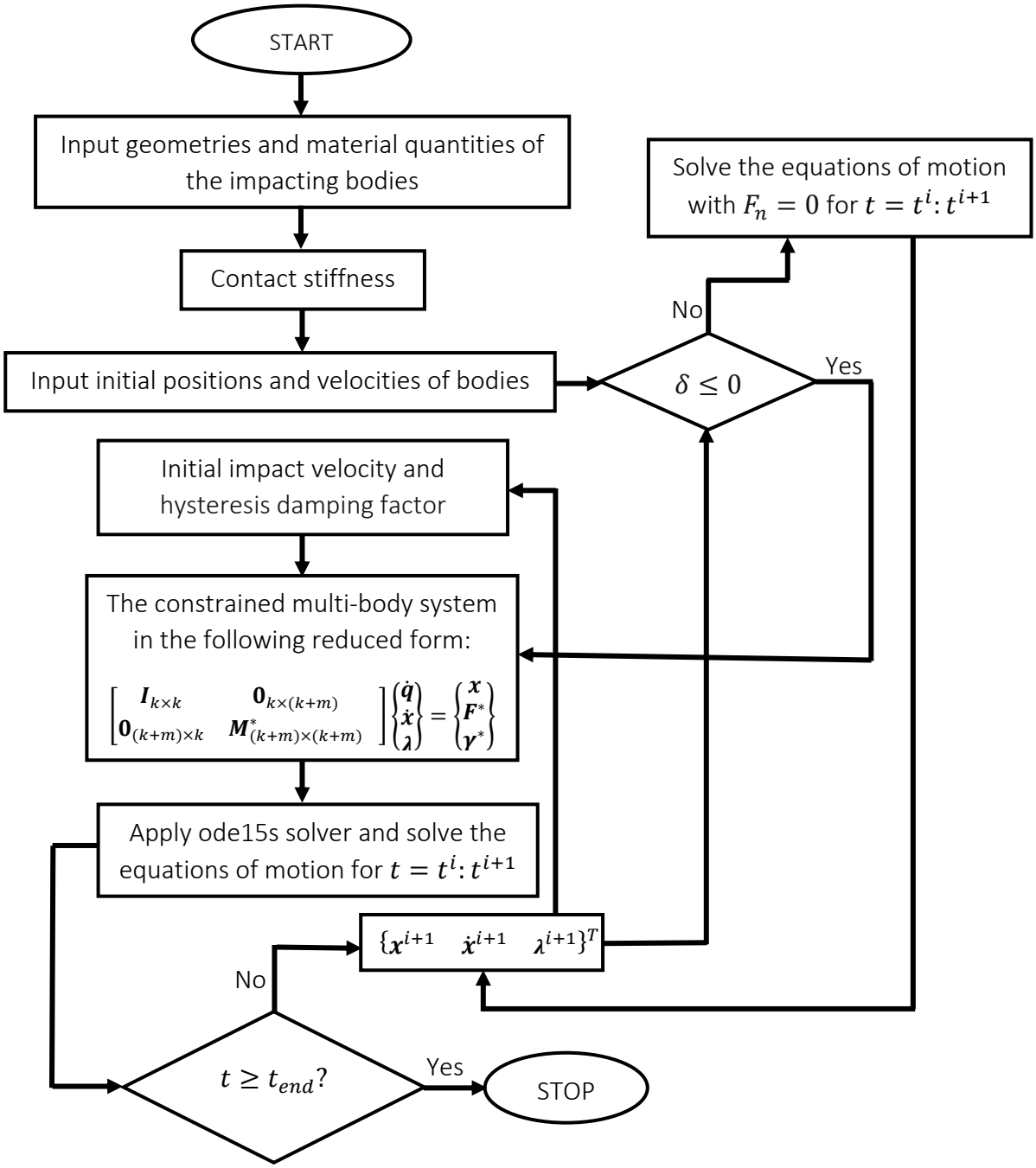
START
Input geometries and material quantities of the impacting bodies
Contact stiffness
Input initial positions and velocities of bodies
Solve the equations of motion with $F_n = 0$ for $t = t^i : t^{i+1}$
No
Yes
$\delta \leq 0$
Initial impact velocity and hysteresis damping factor
The constrained multi-body system in the following reduced form:
$\begin{bmatrix} \boldsymbol{I}_{k\times k} & \boldsymbol{0}_{k\times(k+m)} \\ \boldsymbol{0}_{(k+m)\times k} & \boldsymbol{M}^*_{(k+m)\times(k+m)} \end{bmatrix} \begin{Bmatrix} \dot{\boldsymbol{q}} \\ \dot{\boldsymbol{x}} \\ \boldsymbol{\lambda} \end{Bmatrix} = \begin{Bmatrix} \boldsymbol{x} \\ \boldsymbol{F}^* \\ \boldsymbol{\gamma}^* \end{Bmatrix}$
Apply ode15s solver and solve the equations of motion for $t = t^i : t^{i+1}$
$\{\boldsymbol{x}^{i+1} \quad \dot{\boldsymbol{x}}^{i+1} \quad \boldsymbol{\lambda}^{i+1}\}^T$
No
$t \geq t_{end}$?
Yes
STOP

Figure 4

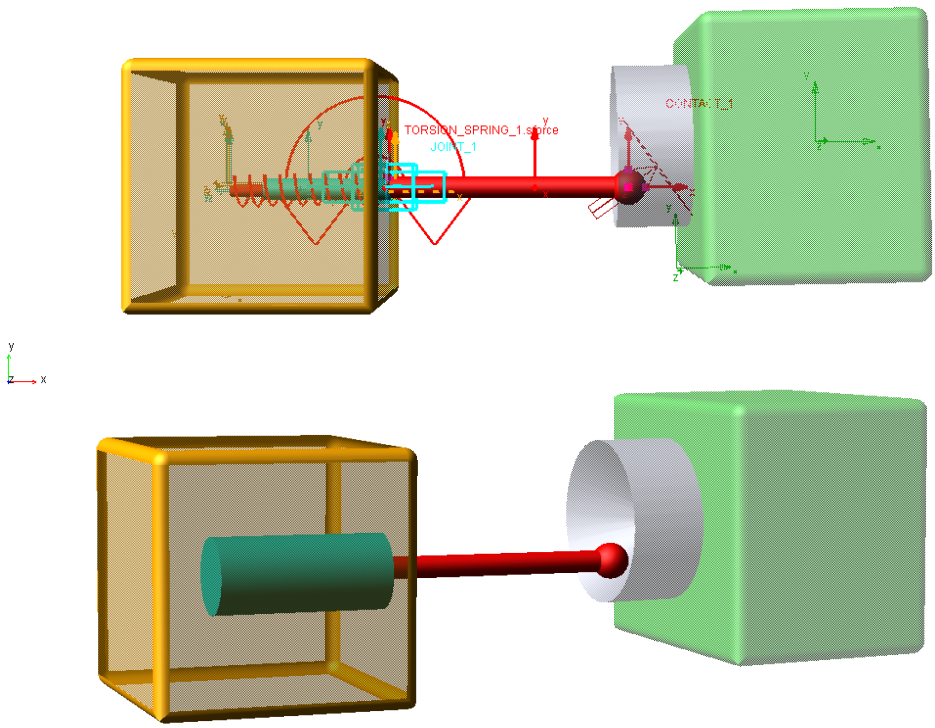

Figure 5

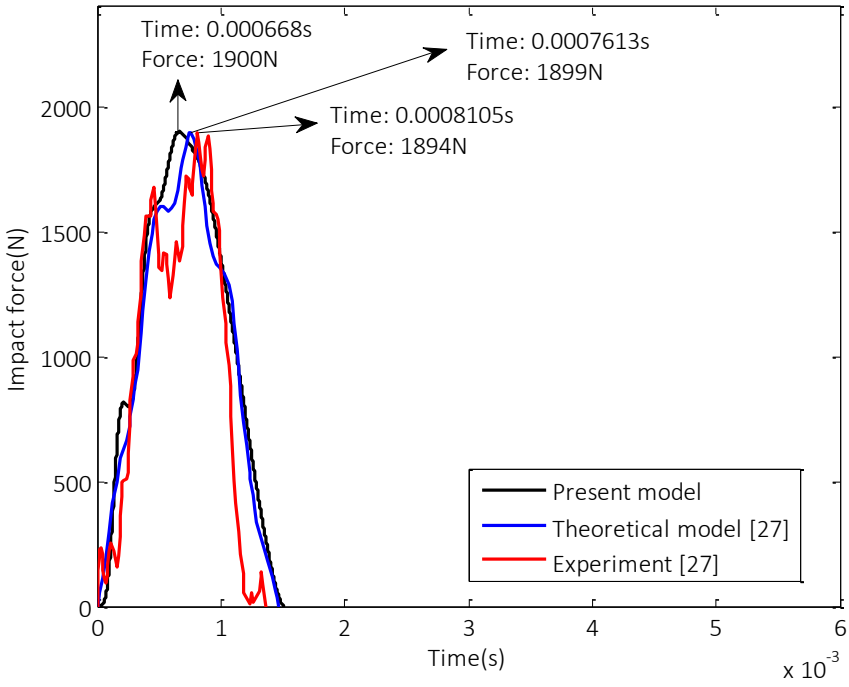
Time: 0.000668s
Force: 1900N
Time: 0.0007613s
Force: 1899N
Time: 0.0008105s
Force: 1894N
Impact force(N)
Time(s)
x 10^-3
Present model
Theoretical model [27]
Experiment [27]

Figure 6

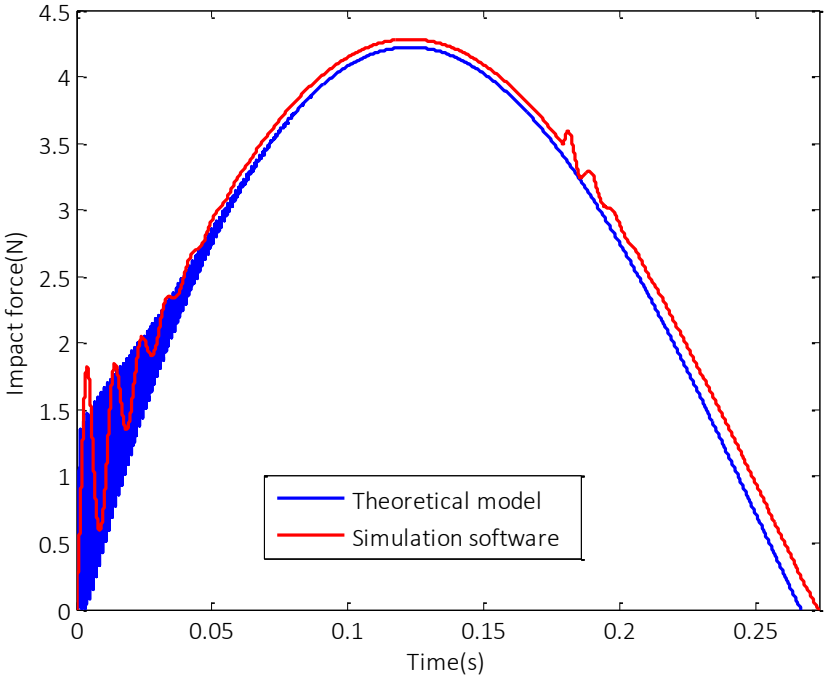
4.5
4
3.5
3
2.5
2
1.5
1
0.5
0
Impact force(N)
0
0.05
0.1
0.15
0.2
0.25
Time(s)
Theoretical model
Simulation software

Figure 7

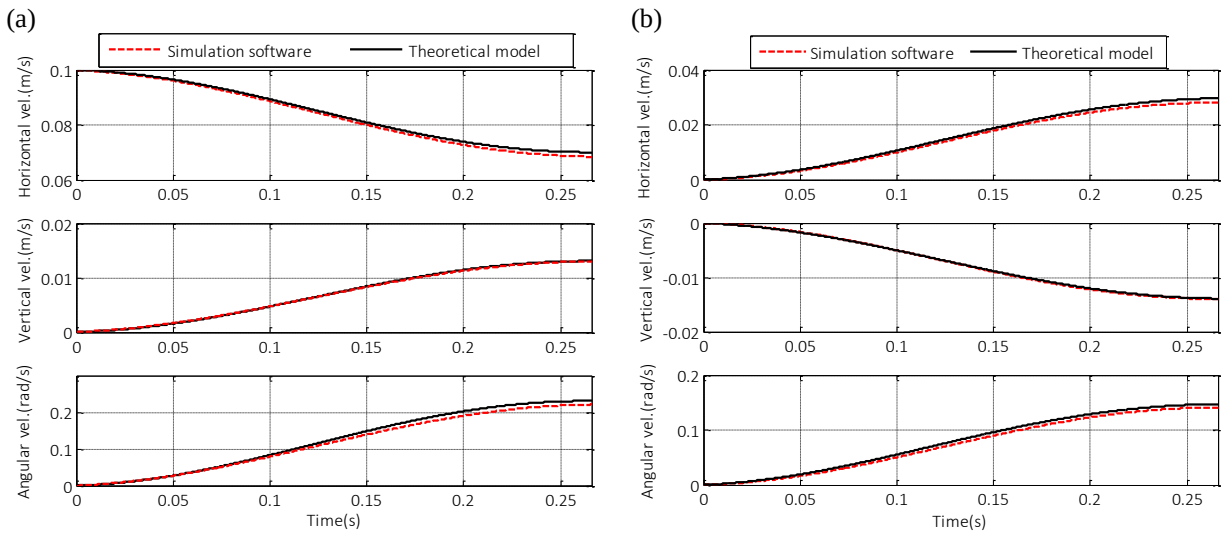
(a)
(b)
Simulation software
Theoretical model
Horizontal vel.(m/s)
Vertical vel.(m/s)
Angular vel.(rad/s)
Time(s)

Figure 8

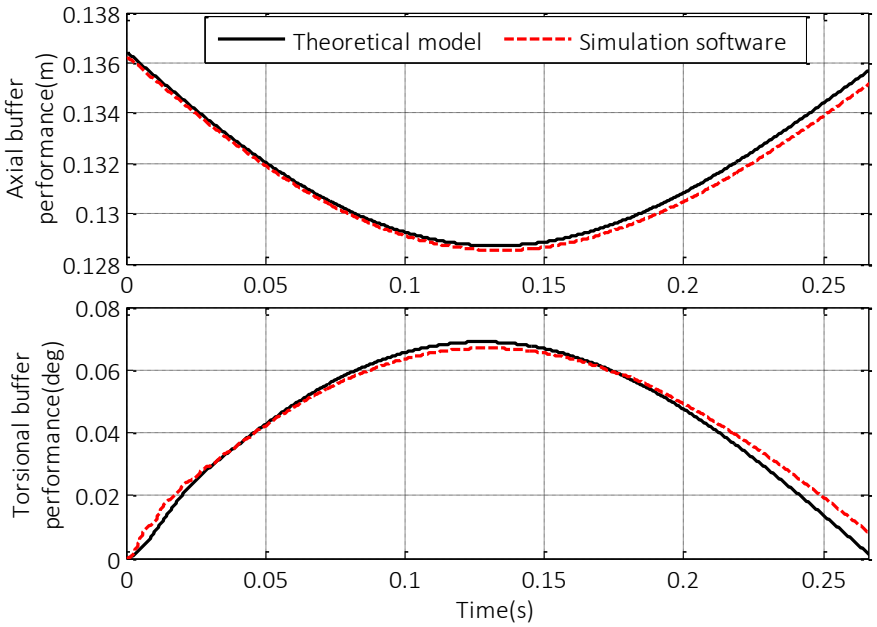
Theoretical model
Simulation software
Axial buffer performance(m)
0.138
0.136
0.134
0.132
0.13
0.128
0
0.05
0.1
0.15
0.2
0.25
Torsional buffer performance(deg)
0.08
0.06
0.04
0.02
0
Time(s)

Figure 9

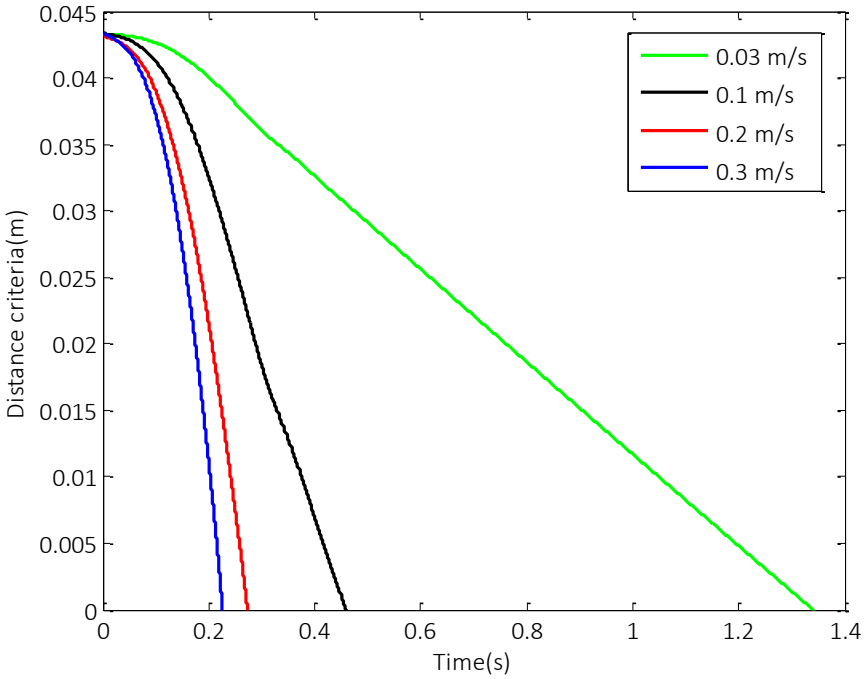
0.03 m/s
0.1 m/s
0.2 m/s
0.3 m/s
Distance criteria(m)
Time(s)
0.045
0.04
0.035
0.03
0.025
0.02
0.015
0.01
0.005
0
0
0.2
0.4
0.6
0.8
1
1.2
1.4

Figure 10

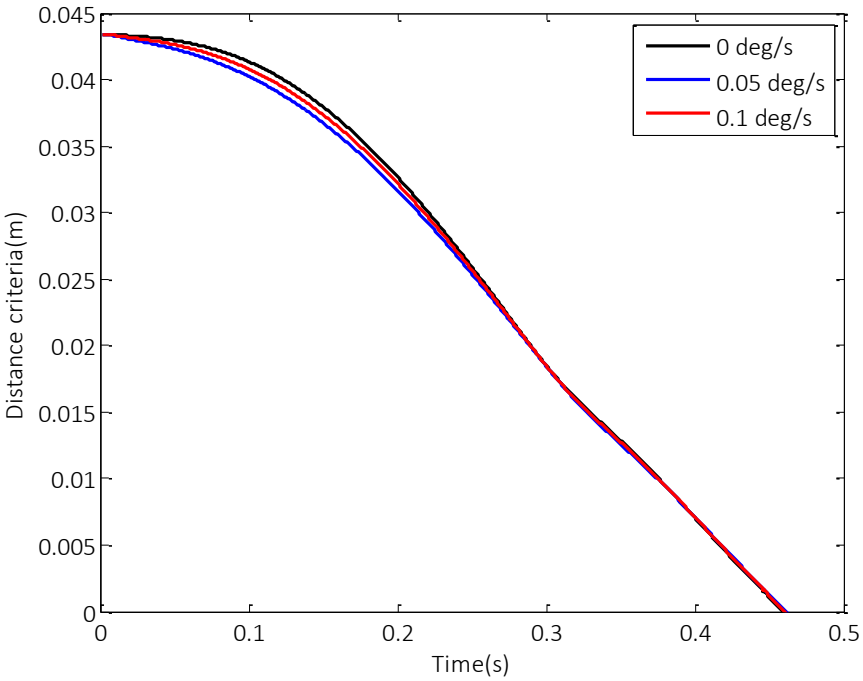
0 deg/s
0.05 deg/s
0.1 deg/s
Distance criteria(m)
Time(s)
0.045
0.04
0.035
0.03
0.025
0.02
0.015
0.01
0.005
0
0
0.1
0.2
0.3
0.4
0.5

Figure 11

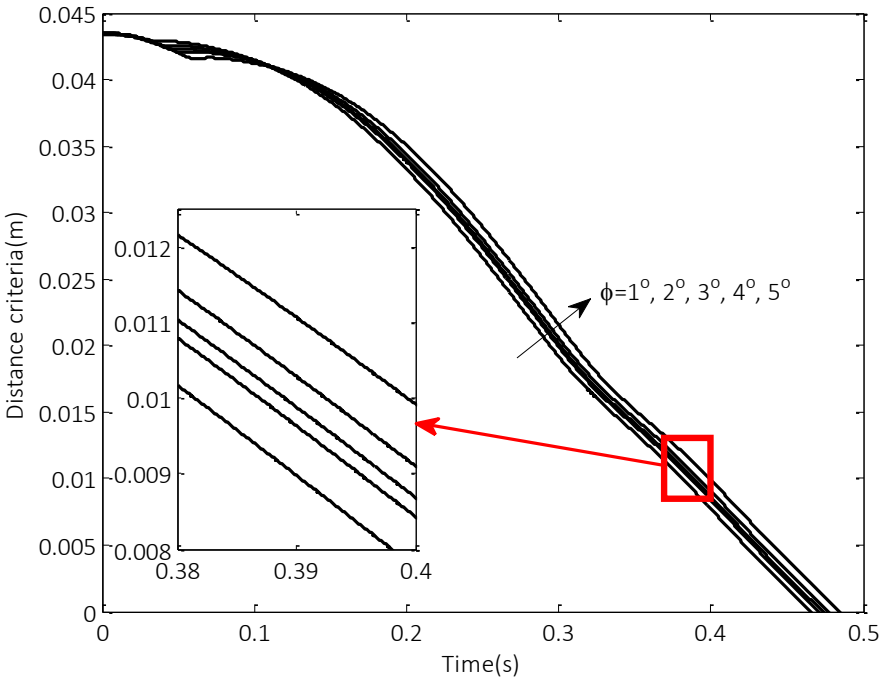
0.045
0.04
0.035
0.03
0.025
0.02
0.015
0.01
0.005
0
Distance criteria(m)
0
0.1
0.2
0.3
0.4
0.5
Time(s)
0.012
0.011
0.01
0.009
0.008
0.38
0.39
0.4
ϕ=1°, 2°, 3°, 4°, 5°

Figure 12

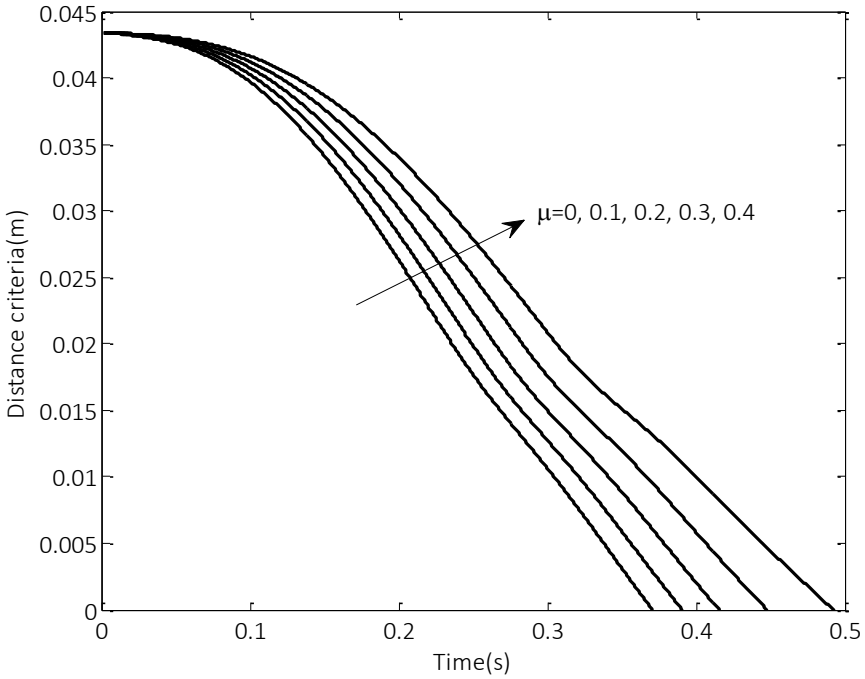
0.045
0.04
0.035
0.03
0.025
0.02
0.015
0.01
0.005
0
Distance criteria(m)
μ=0, 0.1, 0.2, 0.3, 0.4
0
0.1
0.2
0.3
0.4
0.5
Time(s)

Figure 13

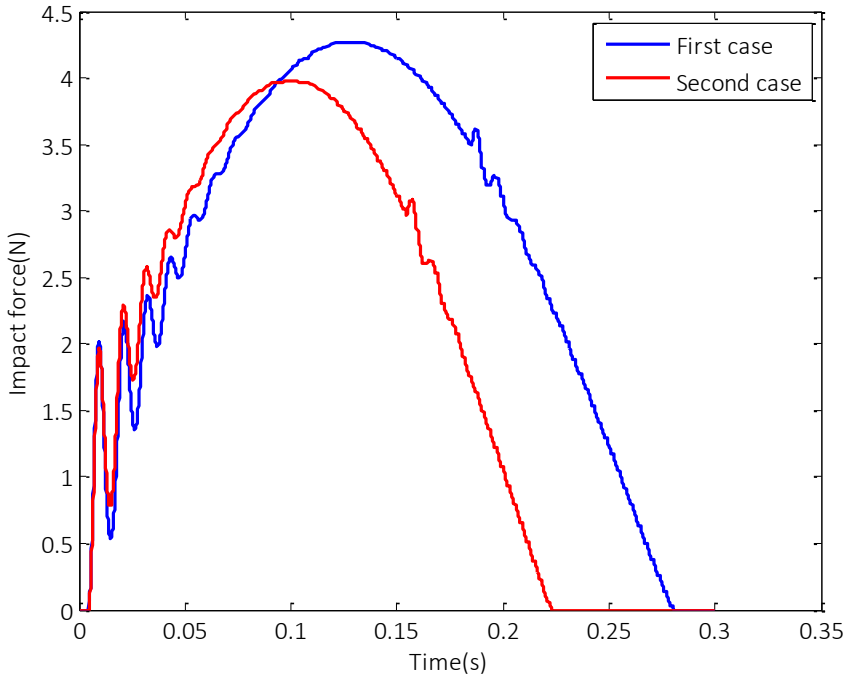
First case
Second case
Impact force(N)
Time(s)
0
0.5
1
1.5
2
2.5
3
3.5
4
4.5
0
0.05
0.1
0.15
0.2
0.25
0.3
0.35

Figure 14

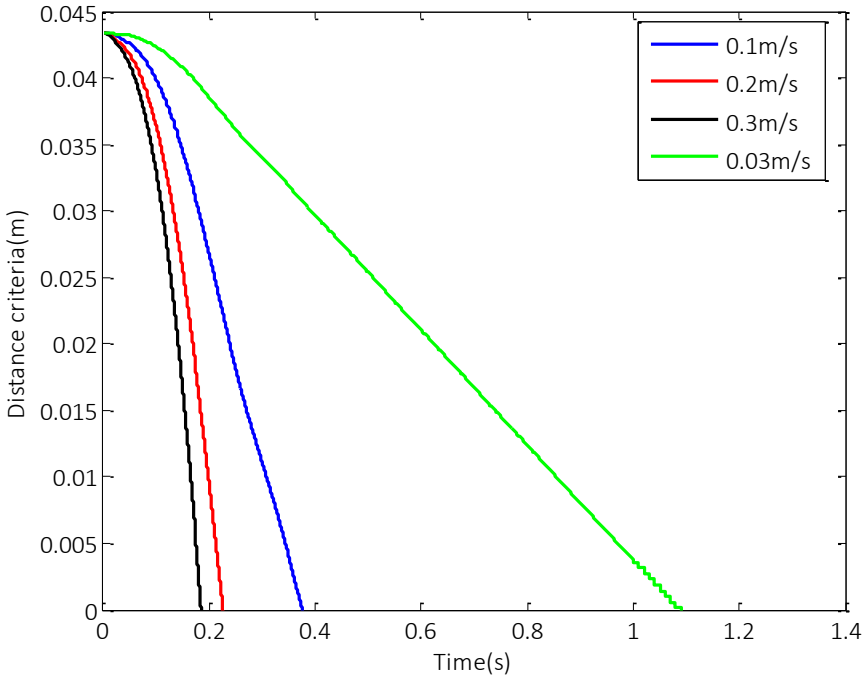
0.045
0.04
0.035
0.03
0.025
0.02
0.015
0.01
0.005
0
Distance criteria(m)
0
0.2
0.4
0.6
0.8
1
1.2
1.4
Time(s)
0.1m/s
0.2m/s
0.3m/s
0.03m/s

Figure 15

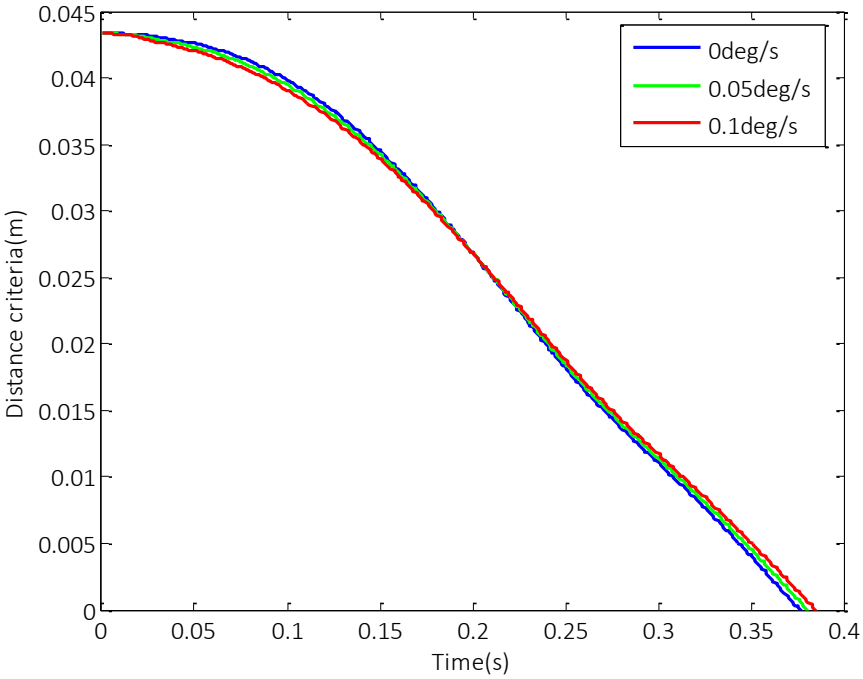
0deg/s
0.05deg/s
0.1deg/s
Distance criteria(m)
Time(s)
0.045
0.04
0.035
0.03
0.025
0.02
0.015
0.01
0.005
0
0
0.05
0.1
0.15
0.2
0.25
0.3
0.35
0.4

Figure 16

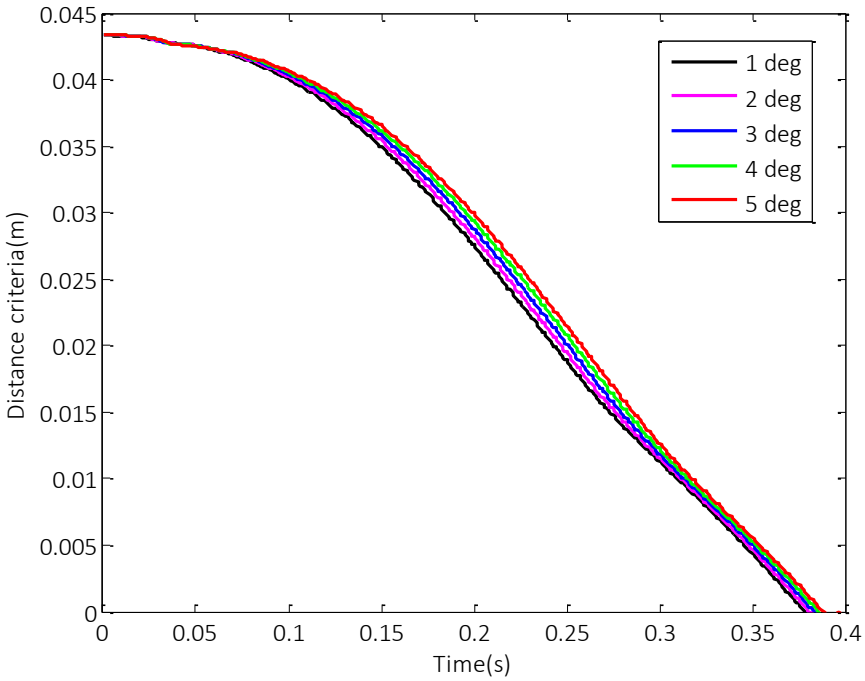
0.045
0.04
0.035
0.03
0.025
0.02
0.015
0.01
0.005
0
Distance criteria(m)
0
0.05
0.1
0.15
0.2
0.25
0.3
0.35
0.4
Time(s)
1 deg
2 deg
3 deg
4 deg
5 deg

Figure 17